Is hazard resilience sustainable?
Evaluating multi-objective outcomes from enhanced seismic design decisions for buildings

Sarah J. Welsh-Huggins[1*] and Abbie B. Liel[2]

[1]Associate Prof., Dept. of Civil, Env. and Arch. Engineering, University of Colorado Boulder
[2] Ph.D. Candidate, Dept. of Civil, Env. and Arch. Engineering, University of Colorado Boulder
*Corresponding author. Email: sarah.welshhuggins@colorado.edu

Abstract

This study investigates the idea that "green" buildings should be designed to withstand higher extreme loads (*i.e.* loads associated with earthquakes or other hazards), to reduce environmental impacts associated with post-hazard repairs. The paper assesses the seismic performance and associated environmental impact of 30 modern reinforced concrete buildings with varying lateral strengths and ductility capacities, considering 4 and 12-story space and perimeter frames. The results show that construction of stronger or more ductile (above-code) buildings requires higher upfront embodied carbon due to larger structural members. Seismic performance is assessed probabilistically using nonlinear dynamic analysis and seismic losses—economic (dollars) and environmental (equivalent CO_2 emissions)—quantified for post-earthquake damage. The findings suggest that enhanced lateral strength lowers post-earthquake economic costs and embodied carbon compared to weaker code-compliant or below-code designs. However, enhancing ductility capacity does not reduce, and can increase, seismic losses. For high seismic regions, enhanced lateral strength can significantly reduce life-cycle embodied carbon losses, enough to offset the higher upfront embodied carbon from constructing larger structural members.

Introduction

A recent paradigm shift in the structural engineering community recognizes that to design for resilience is to design sustainably. Buildings account for roughly 40% of energy use and 35% of total carbon dioxide (CO_2) emissions in the U.S. (CEC, 2008). As a result, advances in green building design offer the potential to significantly reduce resource and energy usage, and associated environmental impacts. At the same time, resilient design principles have emerged from performance-based engineering, linking building design to desired performance outcomes. Performance-based design seeks to reduce hazard-induced (*e.g.* earthquake) building damage and other consequences (Porter, 2003).

Seeking to connect resilient and sustainable design concepts, recent studies have proposed that "green" buildings should be designed for higher levels of seismic and other extreme loads, in order to reduce environmental impacts associated with post-hazard repairs (Chiu *et al.*, 2013; PCA, 2012; Wei, *et al.*, 2016a; Wei, *et al.*, 2016b). A growing body of work explores the relationship between building design features (*e.g.* steel vs. concrete, construction costs), structural response and damage (*e.g.* story drifts, structural losses), and post-earthquake environmental impacts for various building types and life-cycle analysis boundary scopes (*e.g.* Arroyo *et. al.*, 2015; Bocchini *et. al.*, 2014; Feese *et. al.*, 2014; Hossain & Gencturk, 2014; Sarkisian *et. al.*, 2011). Other studies have examined how design strength and ductility capacity impact the economic component of seismic losses (*e.g.* Anagnos *et al.*, 2016; Goulet *et al.*, 2007; Haselton *et al.*, 2011; Ryan *et al.*, 2009). However, no studies have systematically quantified the environmental impacts associated with enhanced seismic design.

This study quantifies and identifies life-cycle tradeoffs relating environmental impact and enhanced seismic designs for 30 reinforced concrete (RC) buildings with varying base shear strengths and ductility capacities. Quantifying the embodied carbon—*i.e.* greenhouse gas emissions released by building manufacturing, construction and post-earthquake repairs—associated with these design decisions elucidates life-cycle implications for the natural environment and human health from changes in seismic design practice. The study's primary aim is to investigate whether enhancing seismic design is a meaningful tool to achieve jointly "greener" and more resilient buildings.

Background

Joint quantification of building hazard resistance and environmental impacts is a still-growing field of research and practice, but a number of frameworks have been suggested to evaluate building life-cycle impacts for this purpose (*e.g.* Court, *et al.*, 2012; Padgett & Li, 2016; Rodriguez-Nikl, 2015; Welsh-Huggins & Liel, 2016). These frameworks offer similar approaches, adding a "post-hazard" stage to the traditional building life-cycle (construction, operation, demolition, etc.) to quantify extra lifetime environmental impacts from hazard-induced repair/replacement actions.

Previous studies have examined the influence of specific building design decisions on building construction and post-earthquake repair impacts by quantifying CO_2 emissions and economic losses. For example, Hossain & Gencturk (2014) conducted Pareto optimization to minimize member size and reinforcement ratios for two RC buildings, under specific design constraints, one with low initial cost and greater design story drifts, and the other with higher upfront cost and lower drifts. They found that larger seismic losses from the low-cost building incurred much higher environmental impacts than the more expensive building. However, the study also suggested that the overall life-cycle environmental impact of the low-cost building was 40% lower than that of the high-cost building due to lower material volumes used in construction and removed during end-of-life disposal. Wei *et al.* (2016) evaluated tradeoffs between environmental, social, and economic costs associated with seismic losses in a cost-benefit analysis of retrofits to an existing building. The study computed a combined present value of losses by monetizing post-hazard carbon emissions and fatalities. Results showed that the retrofit design with the lowest cost and lowest hazard resistance offered the highest present value benefit.

Likewise, Welsh-Huggins and Liel (2016) indirectly considered the influence of member size and design strength on environmental and seismic performance, analyzing members that were "up-sized" to support green roof systems. That study showed that the buildings with larger roof loads (and hence higher member sizes) experienced more seismic damage during intense shaking, but better withstood low-to-moderate shaking. Damaged buildings with higher roof loads were associated with greater post-hazard CO_2 emissions, due to larger material volumes needed for repair/replacement of larger structural members.

Other studies have investigated how design strength and ductility capacity can impact building performance in terms of economic losses, but not environmental impacts. Ramirez *et al.* (2012) quantified the economic seismic losses for the same buildings assessed in this study and found that enhanced lateral strength can reduce post-earthquake economic costs. That study, however, also suggested that enhanced ductility capacity can increase economic seismic losses for low to mid-rise buildings, due to greater damage to nonstructural components and associated losses. Porter (2016) likewise argued against the prevailing idea to design resilient buildings to be more ductile, but weaker. To the contrary, he suggested that a stronger building is more cost-effective for building owners, based on the results of a San Francisco earthquake scenario. Davis and Porter (2016) further suggested that buildings with greater ductility capacity experience larger permanent structural deformations, which can lead to more costly repairs. Those studies pointed to a public desire for building functionality beyond provision of life-safety, which may not be achieved by a design focused on providing ductility.

Case study building designs

Structural design

This study considers a range of structural configurations for special RC perimeter and space moment frames, divided into two design sets. The first set varies by design lateral strength (herein called the "strength design" set), while the second set varies by ductility capacity (the "ductility design" set). Ductility capacity is computed from pushover analysis (described below), following calculations similar to those employed elsewhere (FEMA, 2009). The ductility capacity is defined here as the ratio of post-capping deformation capacity (indicated by the roof drift ratio at which 20% of the lateral strength of the structure has been lost) to yield deformation capacity in terms of roof drift ratio. In all other aspects, each building is code-conforming (ACI, 2011; ASCE, 2010; ICC, 2009). Design parameters for both building sets are listed in Table 1.

The structural designs of the study's modern 4 and 12-story office buildings are adopted from Haselton *et al.* (2011). Each building has a 120 ft. by 180 ft. (36.6 m. by 54.9 m.) footprint. In each direction, the space frames have six lateral load-resisting RC frame lines, while the perimeter frames have two. Column dimensions are the same for interior and exterior space frame lines, while the perimeter frames use smaller square gravity columns at interior columns measuring 12.5 in. (0.32 m.). The first-story height of all buildings is 15 ft. (4.6 m.); all others are 13 ft. (4.0 m.); column spacing is 30 ft. (9.1 m.). The buildings are in Seismic Design Category D, based on a Los Angeles site location, with a design spectral acceleration for short periods of 1.0g and 0.6g at 1 s (ASCE, 2010). All buildings have 8 in. (20.3 cm.) concrete floor slabs.

For the strength design set, the response modification coefficient or "R factor", an inverse modifier on design strength, is changed for each structure. U.S. design standards specify $R = 8$ for special RC moment frames (ASCE, 2010). The strength design set includes buildings weaker than code requirements ($R > 8$) and buildings that are stronger ($R < 8$). For the ductility design set, the design strong-column-weak-beam (SCWB) ratio is varied. For a special moment frame, ACI 318 requires that the sum of column moment strengths at each joint exceed 1.2 times the sum of beam strengths (ACI, 2011). This provision promotes distribution of inelastic structural response over multiple stories, enhancing deformation capacity of the structure (Moehle, *et al.*, 2008). Here, we consider design SCWB ratios ranging from 0.4 to 3.0. Design for above-codes seismic parameters (lower R or higher SCWB ratios) requires larger member sizes and more reinforcing steel. Certain building designs (indicated in Table 1) require greater concrete compressive strengths to satisfy target strengths or ductility capacities.

The 4-story buildings results are the primary focus of this paper. Examples of the 12-story results are described briefly in each section to illustrate the effect of building height on the results.

Architectural design

The inventory of nonstructural building components are based on typical office buildings quantities provided by the SP3 loss estimation software (Haselton Baker Risk Group, 2016). These quantities vary depending on building occupancy type and gross building area. The nonstructural components considered here are: staircases; exterior glazed curtain walls; exterior concrete cladding; interior wall partitions; suspended ceiling tiles; carpeted floor tiles; concrete roof tiles; HVAC ducts; hot and cold water pipes; sanitary waste pipes; and fire sprinkler systems. The quantities and distribution of nonstructural components are the same for buildings of the same height such that only structural member dimensions and quantities vary between building designs.

Embodied carbon associated with upfront construction

Life-cycle analysis (LCA) quantifies potential economic and environmental impacts of a material, product, or system over a given period of time (Hendrickson, Horvath, Joshi, & Lave, 1998). In this study, we assess life-cycle environmental impacts with respect to the amount of *embodied carbon* produced at different stages of the building lifespan. Embodied carbon is the total amount of greenhouse gas emissions, converted to CO_2 equivalents, required to produce a given material or building product (Hammond & Jones, 2008). CO_2 equivalents account for the contribution of various greenhouse gas emissions to climate change. We estimate the main input and output flows of energy/materials (*e.g.* emissions) through a process-based life-cycle analysis of each functional unit of analysis (EPA, 2008), *i.e.* each study building. We use the *SimaPro* software to organize life-cycle inventory quantities from the Ecoinvent database to calculate building life-cycle environmental impacts (Goedkoop, *et al.*, 2013). The Tool for the Reduction and Assessment of Chemical and other Environmental Impacts (TRACI) is used to quantify resulting impacts from raw emissions associated with each inventory process (EPA, 2008).

The building life-cycle stages assessed here are: 1) material manufacturing/production for upfront (pre-service life) building construction, and 2) material manufacturing for post-earthquake building repairs or replacement. The life-cycle environmental impact analysis is conducted for only the upfront and post-hazard material manufacturing because environmental impacts from other stages, *e.g.* on-site construction activities or building operations/routine maintenance actions, are assumed equal for each building, regardless of the structural design. Material transportation to the construction site could produce variations in building life-cycle impacts, depending on the type of vehicle used or volume of structural materials transported, but quantification of these impacts is beyond the scope of the current study. Quantification of demolition/debris removal impacts is also excluded, as is consideration of sources of uncertainty in emissions inventory data.

Upfront embodied carbon for a building is computed from the embodied carbon associated with material manufacturing of all structural and nonstructural building components. The upfront embodied carbon of the nonstructural members is the same for all buildings of the same height, but the structural member contribution to embodied carbon depends on the member sizes, quantity of steel reinforcing, and required concrete compressive strength. Higher concrete strength requires greater quantities of Portland cement, which increases concrete’s unit embodied carbon impact.

This effect is accounted for here with a multiplier on the embodied carbon impact of normal strength concrete (5,000 psi), based on calculations by Hammond and Jones (2006, 2008).

Table 1 presents the upfront embodied carbon for all 30 buildings in this study. Consistent with Guggemos and Horvath (2005), we find that production of structural materials releases higher levels of greenhouse gas and other emissions than production of nonstructural component materials. Fig. 1a shows how upfront embodied carbon varies with lateral strength, such that stronger buildings are associated with greater upfront embodied carbon. Levels of embodied carbon do not correlate linearly with enhanced lateral strength due to other design requirements (gravity loads, drift limits *etc.*) that also impact member sizes, especially at lower lateral load levels. In Fig. 1b, the below-code ductility design buildings have similar levels of upfront embodied carbon. Changes in design SCWB and ductility capacity are associated with redistribution of material from columns to beams without adding much extra material. However, Fig. 1b also demonstrates a notable increase in embodied carbon for buildings with above-code ductility capacities, due to associated increases in member size and steel required to achieve SCWB ratios greater than 2.0.

Nonlinear modeling and dynamic analyses

Nonlinear structural modeling

Two-dimensional, three-bay models of the study buildings were built in the *OpenSEES* seismic analysis program (PEER, 2014). Beam-columns are modeled with elastic elements and concentrated hinge springs, *i.e.* a lumped plasticity approach. These hinges have been assigned a material model capable of capturing concrete spalling and rebar buckling effects at large deformations (Ibarra, *et al.*, 2005). The hinge model also captures cyclic deterioration and accounts for bond-slip. The hinge properties have been calibrated to experimental results of over 250 concrete columns, such that modeling of different components represents differences in design and detailing (Haselton, Liel, Taylor-Lange, & Deierlein, 2016). The models also capture P-Δ effects. The perimeter frame models do not consider the strength and stiffness of the interior (gravity) framing. Rayleigh damping of 5% is applied to the models' first and third modes and assigned only to elastic elements. Haselton and Deierlein (2007) and Haselton *et al.* (2011) provide further details about the structural modeling approach.

Nonlinear static pushover analysis of the buildings verifies that the models exhibit the desired changes in base shear strength and ductility capacity. Fig. 2a presents the pushover results for the 4-story strength design space frames, showing that greater design loads increases the base shear capacity, while ductility capacity remains similar. Increasing the SCWB ratio enhances ductility capacity, as well as base shear strength, as shown in Fig. 2b. Although not shown, the trends are similar for the perimeter frames and 12-story buildings.

Table 1 presents the fundamental period, ultimate base shear strength, and ductility capacity for all buildings. The larger member sizes of the stronger, more ductile designs lead to decreased fundamental periods. Overstrength (the ratio of ultimate to design lateral strength) ranges from 1.6 to 4.3 for the 4-story buildings and from 1.6 to 3.2 for the 12-story buildings. The weaker buildings have higher overstrengths due to gravity loads and other design considerations.

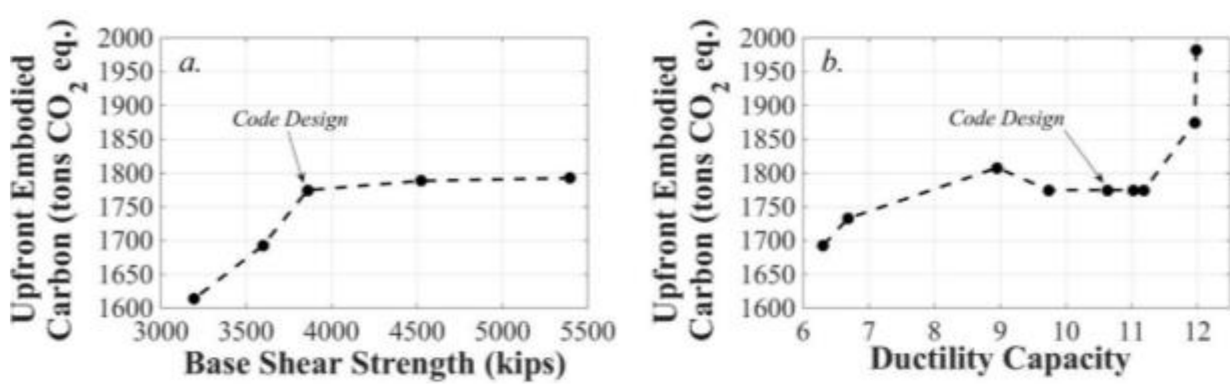

Fig. 1. Influence of seismic design on upfront embodied carbon showing a) effect of ultimate base shear strength for 4-story strength design space frames and b) effect of ductility capacity for 4-story ductility design space frames. (1 kip. = 4,448 N.; 1 ton = 987 kg.).

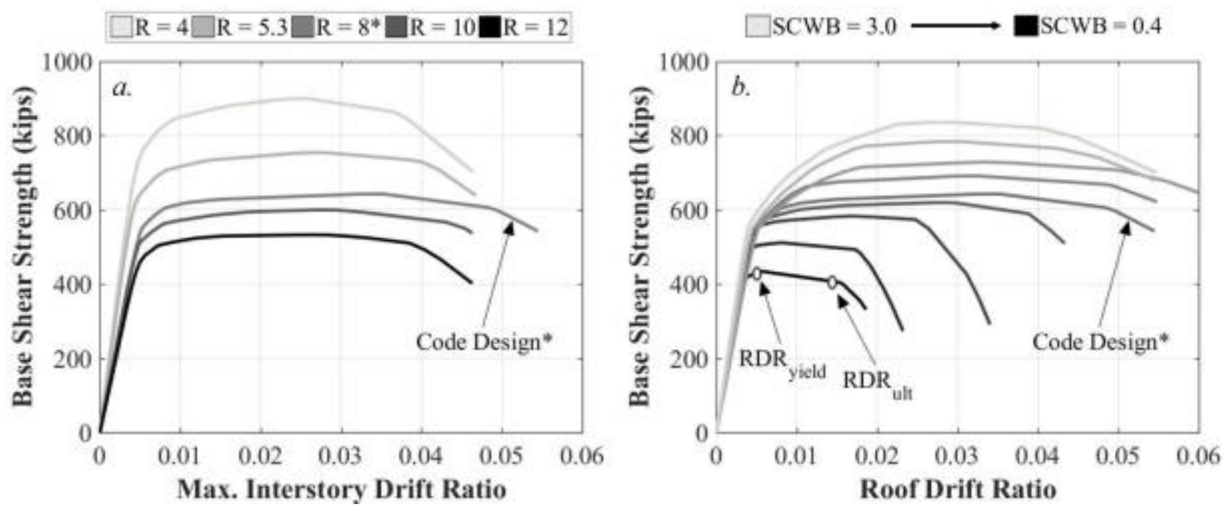

Fig. 2. Nonlinear static pushover results (per frame line) for 4-story a) strength design space frames and b) ductility design space frames. (1 kip. = 4,448 N.). The labels RDR_{yield} and RDR_{ult} on Fig. 2.b) demonstrate the points used to calculate the ductility capacity for a selected building design. RDR_{yield} refers to the roof drift ratio at the maximum lateral strength capacity achieved by a building, while RDR_{ult} refers to the roof drift ratio at which 20% of the lateral strength has been lost for a design.

Dynamic analysis results

The seismic performance of the case study buildings is computed with Incremental Dynamic Analysis (IDA) (Vamvatsikos & Cornell, 2002). In IDA, the building model is subjected to recorded ground motion acceleration time histories. At first, records are scaled to a small value of the spectral acceleration at a building's fundamental period, $Sa(T_1)$, and then structural response is analyzed at increasing scale factors, until collapse is observed. Collapse is defined as occurring when story drifts greater than 12% are recorded at any story, following Haselton *et al.* (2011). The IDA uses a set of thirty strong ground motions recorded from California earthquake, with magnitudes between 6.5-6.9, and at firm sites with site-to-source distances ranging from 15-33 km (Vamvatsikos & Cornell, 2006). These records are representative of the type of crustal ground motions expected at the study site. The seismic hazard analysis for the LA site is obtained from USGS (Petersen et al., 2008) for nine different ground shaking hazard levels, which range from 50% in 50 years, corresponding to an intensity of $Sa(T = 1s) = 0.25g$ (referred to here as Hazard Level 1, or HL 1) to 1% in 50 years (HL 9), associated with $Sa(T = 1s) = 1.25g$. In this study, HLs are defined solely in terms of the spectral acceleration intensity measure and ground motion selection for the study did not consider the influence of spectral shape. Previous analysis results of the same buildings for different ground motions are found in Haselton and Deierlein (2007) and Haselton *et al.* (2011).

The IDA results show that enhanced base shear strength and ductility capacity both increase median collapse capacity (quantified in Table 1 in terms of $Sa(T = 1s)$ for all buildings), compared to code-compliant or below-code designs. Strength designs for the 4 and 12-story perimeter frames and 12-story space frames are highly governed by lateral load demands, making their collapse capacities especially sensitive to design base shear changes. In addition, the below-code 12-story buildings experience damage localization in fewer stories, likely from increased P-Δ effects on weaker, more flexible structures (Haselton & Deierlein, 2007). The buildings designed for enhanced ductility capacity exhibit better collapse performance, as column hinging is prevented and lateral deformation is more evenly distributed along building height (Ramirez et al., 2012).

The IDA results confirm past studies' observations that even subtle design variable changes can strongly affect structural response. Due to the shorter periods of stronger and more ductile buildings, above-code structures dynamically experience larger floor accelerations and smaller story drifts than code-compliant or below-code designs. Perimeter frame design is lateral load-dominated, so base shear strength changes to these buildings have a larger influence on building stiffness and drift and acceleration demands.

Seismic loss results

Probabilistic seismic loss analysis quantifies building performance under seismic loading in terms of building damage and associated seismic losses. The losses are referred to here as *economic costs* (dollar value of post-earthquake component repairs and building replacement) and *embodied* *carbon* (CO_2 equivalents released by post-earthquake material manufacturing for repairs and replacement of damaged components and structures).

Economic costs associated with seismic losses

The seismic loss analysis approach for quantifying post-earthquake economic costs follows the seismic performance and probabilistic loss-estimation procedures developed by the FEMA P-58 project (ATC, 2012a). Here, we have implemented these calculations with SP3, a web-based tool for organizing FEMA-58 loss calculations (Haselton Baker Risk Group, 2016). In this approach, fragility curves quantify the probability that a given structural or nonstructural component is in or exceeds a specified damage state (DS) as a function of the engineering demands on a building, expressed as either peak floor accelerations or story drifts (ATC, 2012a, 2012b). Here, these losses are computed conditioned on a particular hazard level, defined in terms of $Sa(T_1)$. Although the variability and magnitude of these losses may be influenced by the selected intensity measures, this analysis choice is not expected to change greatly the overall comparisons between the different building designs in this study.

The expected seismic loss, $E[SL|HL]$, at each hazard level (shown in Equation 1) is computed as the sum of expected non-collapse building repair costs and total building replacement cost in the case of collapse, considering the collapse probability at that hazard level (ATC, 2012a).

$$E[SL|HL = x_i] = [1 - P(C|HL = x_i)]E[SL|NC, HL = x_i] + P(C|HL = x_i)E[SL|C] \quad \textit{Equation 1}$$

In Equation 1, $P(C|HL = x_i)$ is the probability of collapse at the hazard level (HL) of interest (x_i). $E[SL|NC, HL = x_i]$ is the sum of seismic losses associated with repairing all damaged structural and nonstructural components to restore the building to its initial undamaged state. $E[SL|C]$ is the expected seismic loss (in this section, economic cost) associated with total building replacement resulting collapse. $E[SL|C]$ is assumed to be the same as the cost (or embodied carbon) of initial construction for each building based on typical construction economic costs tabulated by the Haselton Baker Risk Group (2016) and Ramirez *et al.* (2012) and reported in Table 1.

The loss analysis calculations incorporate several thousand Monte Carlo realizations of potential damage outcomes for each structural and nonstructural building component at each hazard level. Each individual realization represents a different level of acceleration and drift, potential damage state entered by the component, and thus varying outcomes for expected non-collapse building repairs costs and total building replacement costs (ATC, 2012a). The number of Monte Carlo realizations varies between analysis of the 4-story and 12-story buildings due to increased computational expense from analyzing a greater number of stories in the taller buildings. For analysis of each building type, the number of Monte Carlo realizations is large enough to ensure that results are not sensitive to this choice.

Fig. 3 shows the median post-earthquake economic costs at each hazard level. The trends presented here are consistent with general observations made in previous studies of the same buildings and other similar designs (Goulet et al., 2007; Ramirez et al., 2012). The strength design buildings in Fig. 3 illustrate a correlation between enhanced lateral strength and decreased economic costs at most hazard levels. In addition, enhanced lateral strength is also associated with greater percent contributions from nonstructural losses due to decreased structural member damage and lower probabilities of collapse. Higher post-earthquake economic costs for stronger buildings at certain hazard levels (*e.g.* 12-story building results in Fig. 3b) arise from the sensitivity of certain nonstructural and structural components to story drifts and floor acceleration demands, which are sensitive to the buildings' fundamental period. This effect is discussed in more detail below.

Table 1. Design variables and seismic analysis outcomes for all 30 case study buildings.

Code Design Parameter	No. Stories/ Frame Type	Upfront Cost/ sq. ft (USD)	Upfront Embodied Carbon (tons CO_2 eq.)	T_1 (sec)[3]	Base Shear Strength (kips)[4]	Ductility Capacity[5]	Median Collapse Capacity $Sa(T = 1s)$ (g)	Post-EQ Economic Cost (Mil. USD)[6]	Post-EQ Embodied Carbon (tons CO_2 eq.)[7]
R = 4	4P[1]	220	2083 *	0.54	5153	21.0	6.70	0.2%	1.6%
R = 8		220	1682 *	1.16	1845	12.5	1.14	7.1%	20.1%
R = 12		220	1439 *	1.15	1393	16.9	0.88	7.4%	22.8%
R = 4	4S[2]	230	1793	0.74	5397	10.5	3.77	2.7%	9.6%
R = 5.3		230	1788	0.78	4526	12.6	3.10	6.1%	17.2%
R = 8		230	1775	0.86	3859	10.6	2.94	8.9%	26.1%
R = 10		230	1693	0.92	3597	10.2	2.31	10.6%	29.0%
R = 12		230	1614	0.97	3196	10.3	1.91	11.0%	30.5%
R = 4	12P	278	5007 **	1.50	2109	2.9	3.36	2.6%	6.2%
R = 8		278	4778 **	2.07	1260	11.9	3.40	4.0%	7.8%
R = 12		278	4500 **	2.93	662	4.6	2.82	8.0%	12.3%
R = 4	12S	291	5739 **	1.93	2409	11.2	2.72	3.2%	1.7%
R = 5.3		291	5728 **	2.11	1911	15.4	2.49	4.7%	7.3%
R = 8		291	5507	2.31	1572	12.9	1.62	5.1%	7.3%
R = 10		291	5318 **	2.38	1288	10.9	1.46	4.6%	6.5%
R = 12		291	5081 **	2.60	1237	10.2	1.19	5.8%	8.5%
SCWB = 3.0	4S	230	1982	0.77	5012	12.0	0.93	9.3%	28.0%
SCWB = 2.5		230	1875	0.82	4701	11.2	0.37	12.9%	36.2%
SCWB = 2.0		230	1775	0.88	4369	12.0	0.09	11.6%	30.4%
SCWB = 1.5		230	1775	0.88	4146	11.0	0.68	11.4%	28.1%
SCWB = 1.0		230	1775	0.86	3714	9.7	0.47	10.9%	24.9%
SCWB = 0.8		230	1693	0.86	3497	9.0	0.32	11.2%	25.5%
SCWB = 0.6		230	1808 *	0.88	3067	6.7	0.24	11.0%	23.1%
SCWB = 0.4		230	1733 *	0.88	2603	6.3	0.22	11.8%	25.0%
SCWB = 3.0	12P	278	5810 *	1.89	1283	22.5	0.71	0.9%	24.7%
SCWB = 2.5		278	5733 *	1.93	1260	20.1	0.60	2.7%	5.6%
SCWB = 2.0		278	5516 *	2.06	1258	13.9	0.46	3.6%	6.8%
SCWB = 1.5		278	5377	2.07	1191	13.1	0.41	3.8%	6.7%
SCWB = 0.9		278	5195 **	2.07	1273	11.9	0.32	27.8%	21.5%

* Entire building designed with concrete compressive strength (f'c) > 5,000 psi 34.5 MPa). ** Bottom stories designed with f'c > 5,000 psi.

[1] "P" denotes perimeter frame design. [2] "S" denotes space frame design.

[3] Period from eigenvalue analysis of simulation models, considering cracked section properties.

[4] Ultimate base shear, for entire building, as determined by nonlinear static pushover analysis (1 kip = 4,448 N).

[5] Period-based ductility capacity as determined by nonlinear static pushover analysis.

[6] Total loss expected over 50 years, discounted at 3%, normalized by total building replacement cost.

[7] Total loss expected over 50 years, discounted at 0%, normalized by total building replacement embodied carbon (1 ton = 987 kg.).

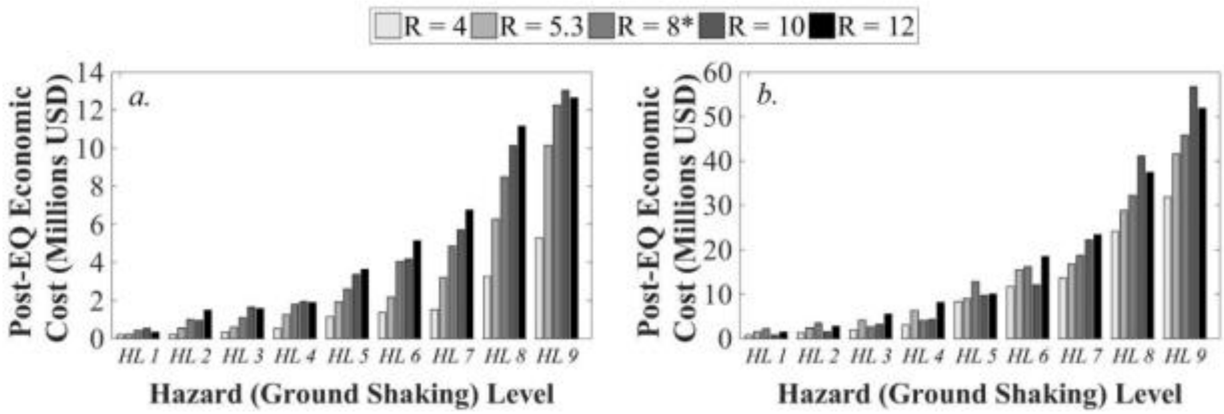

Fig. 3. Median post-earthquake economic cost for strength design space frames for a) 4-story and b) 12-story buildings at each hazard level. (denotes code-compliant designs).*

Enhanced (above-code) ductility capacity, although improving collapse capacity, generally does not reduce economic seismic losses. For the above-code buildings, more even distribution of lateral deformation, due to greater ductility capacity, also increases the percent contribution and magnitude of nonstructural losses. Fig. 4 compares how the percent contribution to total post-earthquake economic cost from non-collapse and collapse seismic losses varies with ductility capacity. The more ductile building (*e.g.* SCWB = 2.5) has significantly lower collapse loss contributions than a below-code, less ductile building (*e.g.* SCWB = 0.6). The below-code building has lower total (collapse plus non-collapse) seismic economic losses at each hazard level, but much larger percent contribution from collapse. The selected 4-story buildings presented in Fig. 4 are representative of the general trends observed for these buildings.

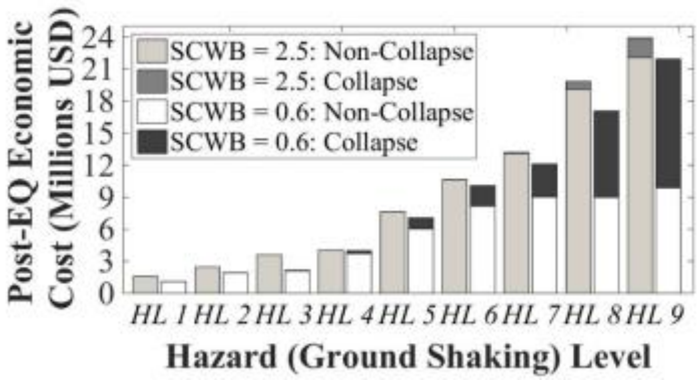

Fig. 4. Post-earthquake economic costs deaggregated by non-collapse and collapse costs at each hazard level for selected 4-story above-code (SCWB = 2.5) and below-code (SCWB = 0.6) ductility design space frames.

We also quantify the expected annualized losses (EAL) for each building. EAL is calculated based on each hazard level's frequency of exceedance and estimated loss (either dollar or, below, CO_2 equivalents) following the analytical EAL solution described by Baker and Cornell (2003). This calculation is presented in Equation 2, where the expected annualized seismic loss considers the magnitude of losses at each hazard level, as well as the likelihood of each hazard level occurring:

$$EAL = \sum\{E[SL|HL = x_i] * \Delta\lambda_{HL}(x_i)\} \qquad \textit{Equation 2}$$

In this case, $E[SL|HL = x_i]$ is the expected seismic loss computed for a given hazard level x_i and $\Delta\lambda_{HL}(x_i)$ is a vector representing the mean frequency of exceedance for each hazard level.

Fig. 5 presents the expected annualized economic costs for selected 4 and 12-story buildings. Increasing lateral strength decreases EAL, regardless of building height. Conversely, enhancing ductility capacity does not necessarily imply lower seismic loss in low- to mid-rise (*e.g.* 4-story) structures, because the distribution of lateral deformation throughout a greater number of building stories increases the magnitude of non-collapse (especially nonstructural) losses in the entire structure. The 12-story ductility designs, however, reverse the trend of their 4-story counterparts, demonstrating lower post-earthquake economic costs with increasing ductility capacity, due to more localized damage in taller buildings.

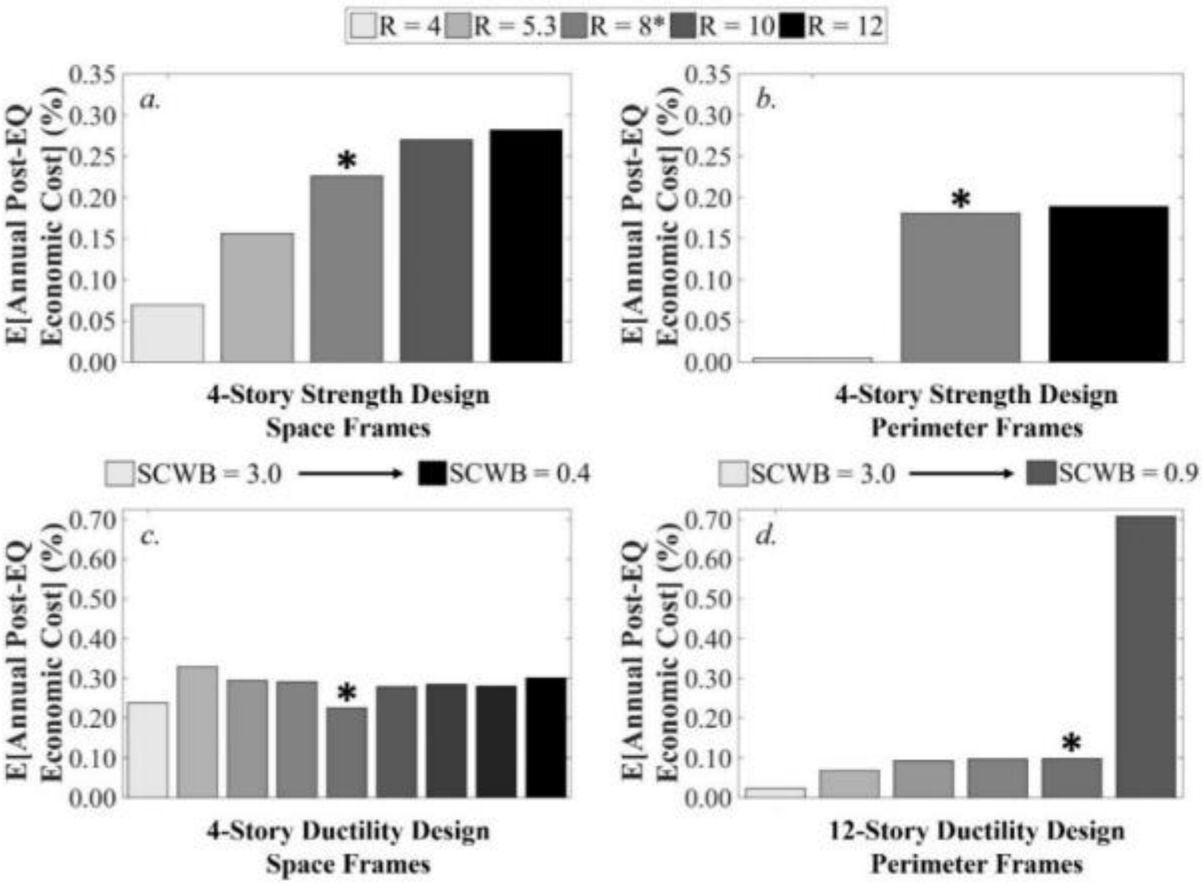

Fig. 5. Expected annual post-earthquake economic cost for 4-story strength design a) space frames, b) perimeter frames, c) 4-story ductility design space frames, and d) 12-story ductility design perimeter frames. Losses are annuities and expressed as percentage of total building replacement cost. (denotes code-compliant designs).*

Embodied carbon associated with seismic losses

Quantification of environmental impacts associated with seismic losses is a still-growing field of research. This study links seismic damage to the embodied carbon associated with manufacturing the materials required for potential post-earthquake building repairs. Previous work by the authors (Welsh-Huggins & Liel, 2016) details our approach for translating damaged component quantities into material volumes for specific repair actions at each hazard level. That study cataloged each nonstructural and structural repair action recommended in FEMA P-58 (ATC, 2012b) by material needs and quantities, following typical construction practices described in Ching (2014). Thus, through this approach, at each Monte Carlo realization in the loss analysis, damage states and repair actions are identified for each component in the building, and then the embodied carbon impact from the required repair or replacement materials (*e.g.* structural steel, glass, etc.) is computed (Welsh-Huggins & Liel, 2016). For collapse case, calculation of embodied carbon loss accounts for the lower total replacement embodied carbon quantities (from smaller structural members) of below-code (weaker or less ductile) buildings. We assume that building repairs and replacement will use the same materials/components as in the original construction *(i.e.* no post-hazard event upgrades). The result of these calculations for each building is a lognormal distribution of embodied carbon released by repair/replacement activities at each hazard level.

Fig. 6 presents median post-earthquake embodied carbon at each hazard level for the 4-story strength designs, showing the same general trend as the economic seismic losses. Normalized embodied carbon (median post-earthquake embodied carbon at each hazard level divided by total replacement embodied carbon) is also lower for perimeter frames than for space frames, and lower for taller buildings than for their 4-story equivalents. Although not shown, 4-story ductility design trends in embodied carbon as a function of hazard level differ than those observed for economic losses. The greater magnitude of nonstructural damage for more ductile buildings and lower replacement embodied carbon for less ductile buildings results in higher post-earthquake embodied carbon for above-code ductility designs.

The trends in post-earthquake embodied carbon losses also highlight the influence of fundamental period on structural response and on associated nonstructural component response and damage, particularly for the structures designed to vary by lateral strength. The stronger, stiffer buildings, with lower fundamental periods, experience lower story drifts and higher peak floor accelerations than weaker designs. The response of stiffer buildings is associated with higher nonstructural losses, because the fragility functions of most nonstructural components are acceleration-sensitive (as seen in Fig. 6a). The code-compliant space frame (R = 8) has a slightly higher collapse capacity than the weaker frames, but experiences higher floor accelerations. Therefore, at shaking intensities greater than 10% in 75 years (HL 6), non-collapse repairs for the code-compliant space frame produce more embodied carbon than below-code designs, due to a greater number of damaged nonstructural components that also require more carbon-intensive repair actions or total component replacement, with only somewhat reduced collapse losses.

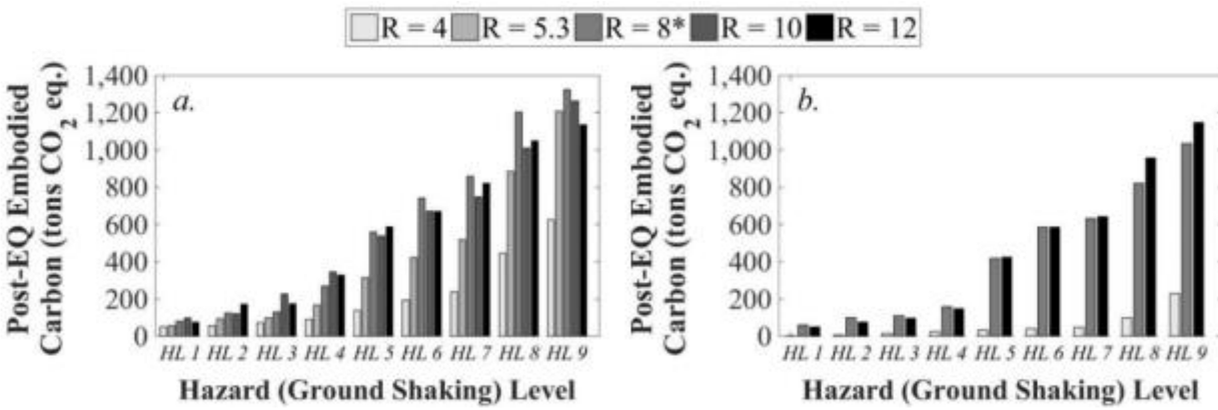

Fig. 6. Median post-earthquake embodied carbon for 4-story strength design a) space frames and b) perimeter frames at each hazard level. (denotes code-compliant designs. 1 ton = 987 kg.)*

Fig. 7 shows that trends in annualized embodied carbon for all 4-story buildings generally follow the observations described above for hazard level loss, *i.e.* stronger buildings have *lower* annualized expected embodied carbon (63% lower than the code-compliant design in the case of the strongest space frame), while more ductile buildings mostly have *higher* expected annual embodied carbon (19% more than the code-level design for the most ductile design). Although not depicted in Fig. 7, the results for the 12-story strength design buildings (presented in Table 1) follow the same trend as their 4-story counterparts. By comparison, the 12-story ductility design results, as shown in Table 1, demonstrate enhancing ductility capacity in taller buildings offers only a limited advantage for reduced post-earthquake embodied carbon. The above-code 12-story ductility designs reduce annual post-earthquake embodied carbon only at SCWB ratios below 3.0; above this SCWB ratio, the higher nonstructural losses for this design result in a post-earthquake embodied carbon impact greater than 3.5 times that of the code-compliant design.

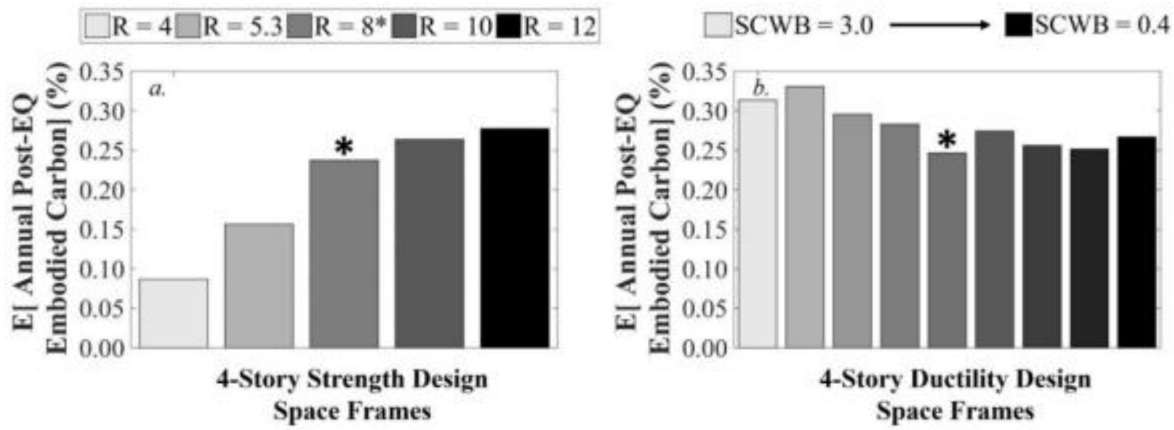

Fig. 7. Expected annual post-earthquake embodied carbon loss for 4-story space frames for a) strength designs and b) ductility designs. Losses are annuities and expressed as percentage of total building replacement embodied carbon values. (denotes code-compliant designs).*

Component-level contribution to seismic losses

Changes in seismic design also affect which building components contribute the most to seismic losses at each hazard level. Here, seismic losses are deaggregated at each of the hazard levels with respect to the contributing component, or so-called "performance groups." The cost of post-collapse total building replacement is defined as its own performance group ("collapse") to evaluate the impact of rebuilding the entire structure as compared to that of repair or replacement of specific damaged components.

Fig. 8 shows component contributions to seismic loss for selected 4-story strength design space frames at each of the considered hazard levels. The left column illustrates post-earthquake economic costs (presented as median values at each hazard level in Fig. 3a) and, in the right column, embodied carbon (median values at each hazard level in Fig. 6a) as percentages of total seismic loss. The dominant building components contributing to seismic loss at each hazard level vary with the analysis metric of interest, due to differences in associated repair cost or CO_2 emissions consequences per damaged unit. In particular, depending on the damage state(s) entered at a hazard level, certain components (such as ceiling tiles, interior partitions, or HCAV ducts) may require more CO_2-intensive repairs than other components with higher economic costs (like beam-columns or exterior concrete cladding). At low to middle hazard levels, relatively expensive repairs to exterior concrete cladding dominate non-collapse economic costs for the above-code 4-story building (HL 5 to HL 8 in Fig. 8a). However, for the same building and hazard levels, embodied carbon contributions are dominated by repair/replacement activities for ceiling tiles and interior partitions. The weakest 4-story building (Fig. 8b) has higher probabilities of collapse (and thus, of total building replacement) at higher levels of shaking, leading to larger contributions from structural repairs and total replacement to both economic cost and embodied carbon seismic losses. Trends are similar for the 12-story strength design set, with greater contribution from full building replacement for taller, below-code buildings than for their 4-story equivalents.

Varying ductility capacity (not shown in Fig. 8) exhibits similar trends in component contribution to seismic losses. At higher hazard levels, however, nonstructural component contribution for the most ductile buildings is larger than for the most above-code strength design 4 or 12-story buildings when either metric is considered. This trend occurs because enhanced ductility is associated with greater water conveyance pipe and HVAC duct damage, and repairs to these components require, for a given floor, significant quantities of steel and member replacement in large interconnected units. As discussed above, selection of a different intensity measure or suite of ground motions could change these results slightly, due to variations in structural and nonstructural member response, but are not expected to influence overall trends in results.

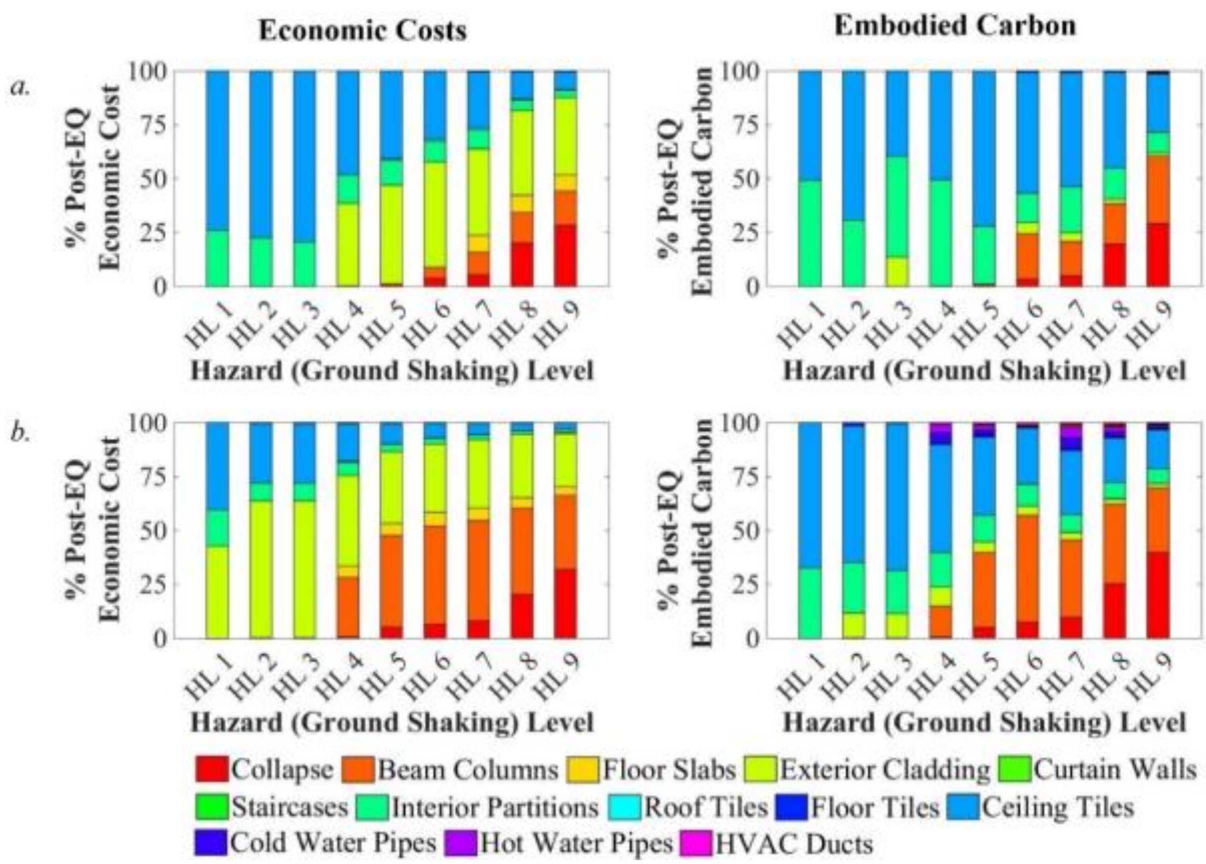

Fig. 8. Deaggregated component contributions to seismic losses in terms of economic costs and embodied carbon loss for 4-story strength design space frames: a) above-code (R = 4), and b) below-code (R = 12), at nine different ground shaking intensities.

Total embodied carbon seismic losses

Computation of the present value of future (*i.e.* uncertain) seismic losses considers present day implications of different seismic design decisions over time. Present value calculations are typically made using engineering economic equations wherein a discount rate is applied to future losses. Applying a discount factor accounts for the time value of money, where costs incurred in the future are valued less than if they occurred today (Cowing, *et al.* 2004); 3% is perhaps the most commonly recommended discount rate in engineering economic analyses (Pate-Cornell, 1984). However, climate change science questions the ethics of applying discount factors for total calculation of non-monetary metrics like carbon emissions. Consequently, many scholars recommend either no or a very low discount rate for environmental impact present value analysis

(Jacquet, *et al.* 2013; Schelling, 1995; Tol, 2011). We address this concern regarding present value discounting of environmental impacts by first computing present value (total) post-earthquake embodied carbon loss at four different discount rates from the annualized losses. The present value seismic loss is computed in terms of the CO_2, not dollar, equivalents of embodied carbon to avoid discussion of appropriate economic valuation of future carbon emissions. A 50-year building service life is assumed for these calculations.

Fig. 9 shows how total post-earthquake loss decreases as discount rate increases, implying that higher discount rates decrease the value placed on future societal impacts from embodied carbon. In addition, for both design sets, increasing the discount rate has more effect on embodied carbon losses of a higher magnitude, *i.e.* generally associated with the weaker buildings, thus reducing the relative importance of those losses when compared to stronger buildings. However, for the reasons described above, the remainder of this study assumes a 0% discount rate (essentially the sum of embodied carbon annuities over 50 years), for computing total embodied carbon losses and also assumes a 3% discount rate when computing the economic losses.

Fig. 9 compares the influence of base shear strength and ductility capacity on present value post-earthquake embodied carbon. As shown previously in Fig. 1, upfront embodied carbon increases with enhanced strength or ductility capacity. However, consistent with the seismic loss analysis, total post-earthquake embodied carbon decreases with enhanced lateral strength. For these 4-story space frames, upfront material production for the most above-code strength design releases 18 more tons (16,300 kg) of CO_2 equivalents than upfront material production for the code-level design. However, at a 0% discount rate, post-earthquake repair/replacement activities for the same enhanced design releases 133 fewer tons of CO_2 equivalents (120,660 kg) than the code-compliant design, indicating a net reduction when both upfront and total post-earthquake

CO_2 are considered. This result supports an idea posited by the Portland Concrete Association that one tool for achieving "greener" buildings is to design for expected seismic forces 20% higher than required by current standards (PCA, 2012). Shown in Fig. 10, a 20% increase in strength leads to significant savings in avoided embodied carbon due to lower seismic losses, compared to the original code-compliant design. These analyses (also generalizable to the 12-story designs) demonstrate that increased upfront embodied carbon for enhanced lateral strength can be offset by significant reductions in future post-earthquake embodied carbon from lower seismic losses.

However, enhanced ductility capacity can increase total post-earthquake embodied carbon Fig. 9b. Results for the ductility designs assessed in this study suggest that, depending on building height and desired ductility capacity, above-code designs can increase both upfront embodied carbon (from larger structural member sizes to achieve enhanced SCWB ratios) and total seismic loss embodied carbon (due to greater nonstructural damage). Even in cases where the post-earthquake embodied carbon decreases with enhanced ductility, this reduction is not sufficient to counteract the additional upfront carbon produced from the above-code designs.

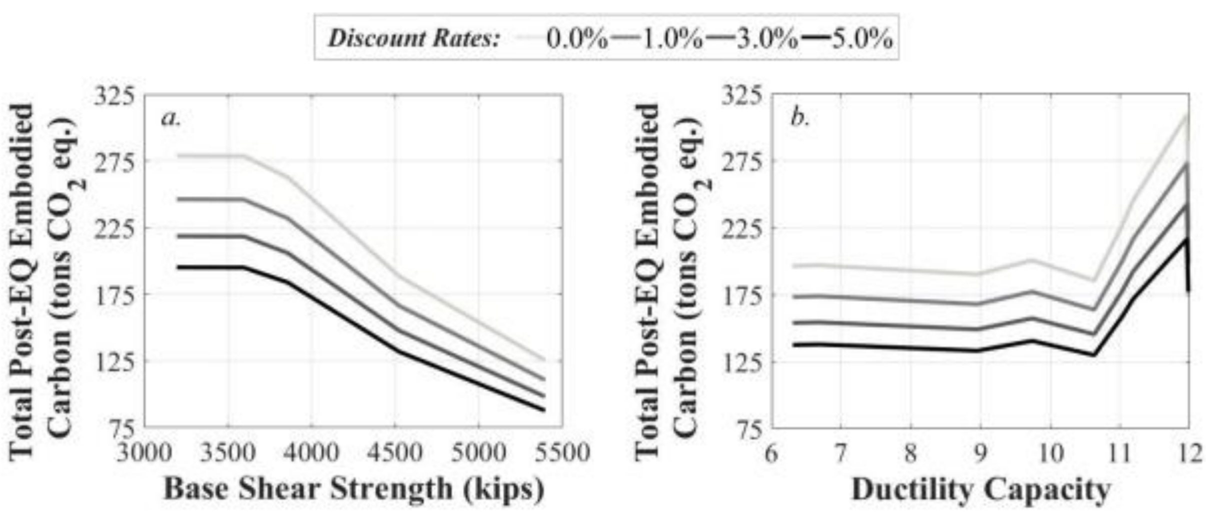

Fig. 9. Total post-earthquake embodied carbon for 4-story space frames with respect to a) base shear strength for strength designs, and b) ductility capacity for ductility designs, showing the effect of discount rate on these calculations.

Influence of seismic hazard on embodied carbon seismic losses

The relative influence of enhanced seismic design also will depend on the geographic region for which a building is designed, due to differences in seismic hazard. Fig. 10 compares the predicted present value of embodied carbon seismic losses, should the 4-story strength design space frames be constructed at sites with higher (Pasadena, CA) or lower (Reno, NV) seismic hazard than at the presumed location in Los Angeles (Petersen et al., 2008). The three locations have the same soil site class (D) and similar fault types.

The results presented in Fig. 10 show that for any of the considered building designs, as expected, lower hazard levels decrease the total embodied carbon associated with seismic losses. It is important to note, however, that code-specifications for lateral strength would vary based on the expected seismic hazard of these different sites, as indicated in the figure by the symbols for expected "code-design" values of base shear strength in Reno and Pasadena. In Pasadena, enhancing lateral strength offers a major reduction in total post-earthquake embodied carbon compared with designing to-code. In Reno, there is smaller difference in post-earthquake embodied carbon from designing above-code or at the code-minimum. These results suggest that for sites with high seismic hazard, increasing a building's design lateral strength can significantly reduce embodied carbon from seismic losses, but this effect will be less significant in areas of lower seismicity.

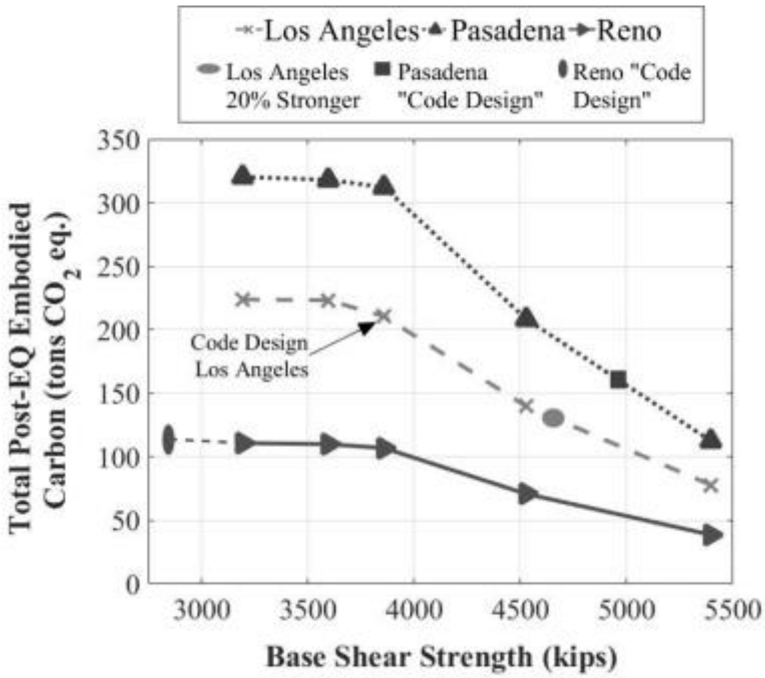

Fig. 10. Influence of ultimate base shear strength on total seismic embodied carbon loss for Los Angeles, CA study site, compared to sites of higher and lower seismic hazard. Expected results for a building with 20% greater design strength in Los Angeles also shown. (1 kip = 4,448 N.; 1 ton = 987 kg.).

Multi-objective analysis of economic and environmental metrics

Multi-objective analysis (MOA) is implemented here to identify and quantify relative strengths and weaknesses of the chosen design variations, across multiple design variable and possible analysis outcome categories. MOA is not used in this study for design optimization, which is already the subject of a number of structural engineering life-cycle assessment and seismic design studies. Rather, in the form employed here, MOA allows us to represent and assess the complexity of real-world decision-making and the nuanced technical, social, economic, and environmental importance inherent to the specific units of measurement of each category (Kajikawa, 2008).

Fig. 11 illustrates the MOA design objectives—upfront embodied carbon, base shear strength, and ductility capacity; and seismic analysis outcomes—collapse capacity, and total economic and embodied carbon seismic losses. Fig. 11a presents the MOA results for the 4-story strength designs, where the results of the code-compliant space frame are used as a baseline case for comparison (shown as the black horizontal line). The figure demonstrates that the above-code (R = 4) strength design building has the most desirable attributes apart from upfront embodied carbon (for which it is slightly less desirable than the above-code, R = 5.3 design). However, the building's higher upfront embodied carbon (73 tons, or approximately 66,000 kg., more CO_2 equivalents than the baseline design) is offset by significant savings in reduced seismic losses. Moreover, the structural design of this building achieves enhanced lateral strength without a major increase in upfront embodied carbon. These and other MOA results suggest that enhanced lateral strength can produce more resilient (higher collapse capacities and lower economic seismic loss) and greener (lower seismic loss embodied carbon) outcomes than a code-compliant design. Moreover, upfront increases in embodied carbon can be offset by avoided post-earthquake impacts, *i.e.* a net reduction in life-cycle embodied carbon, compared to the code-compliant design.

Comparatively, Fig. 11b presents the MOA results with respect to the 4-story ductility design buildings, using the same code-compliant design as a baseline. The challenge of enhancing seismic design through increased ductility capacity is evident in the MOA results for the above-code ductility design space frames (SCWB > 1.2). Although these buildings have higher ultimate base shear strength and improved ductility capacity compared to the baseline design, their complex collapse mechanisms and nonstructural component damage when subjected to large drifts result in much less desirable seismic loss outcomes. Overall, the MOA results shown in Fig. 11b demonstrate that enhancing ductility capacity upfront does not enhance life-cycle embodied carbon or economic costs associated with post-earthquake losses.

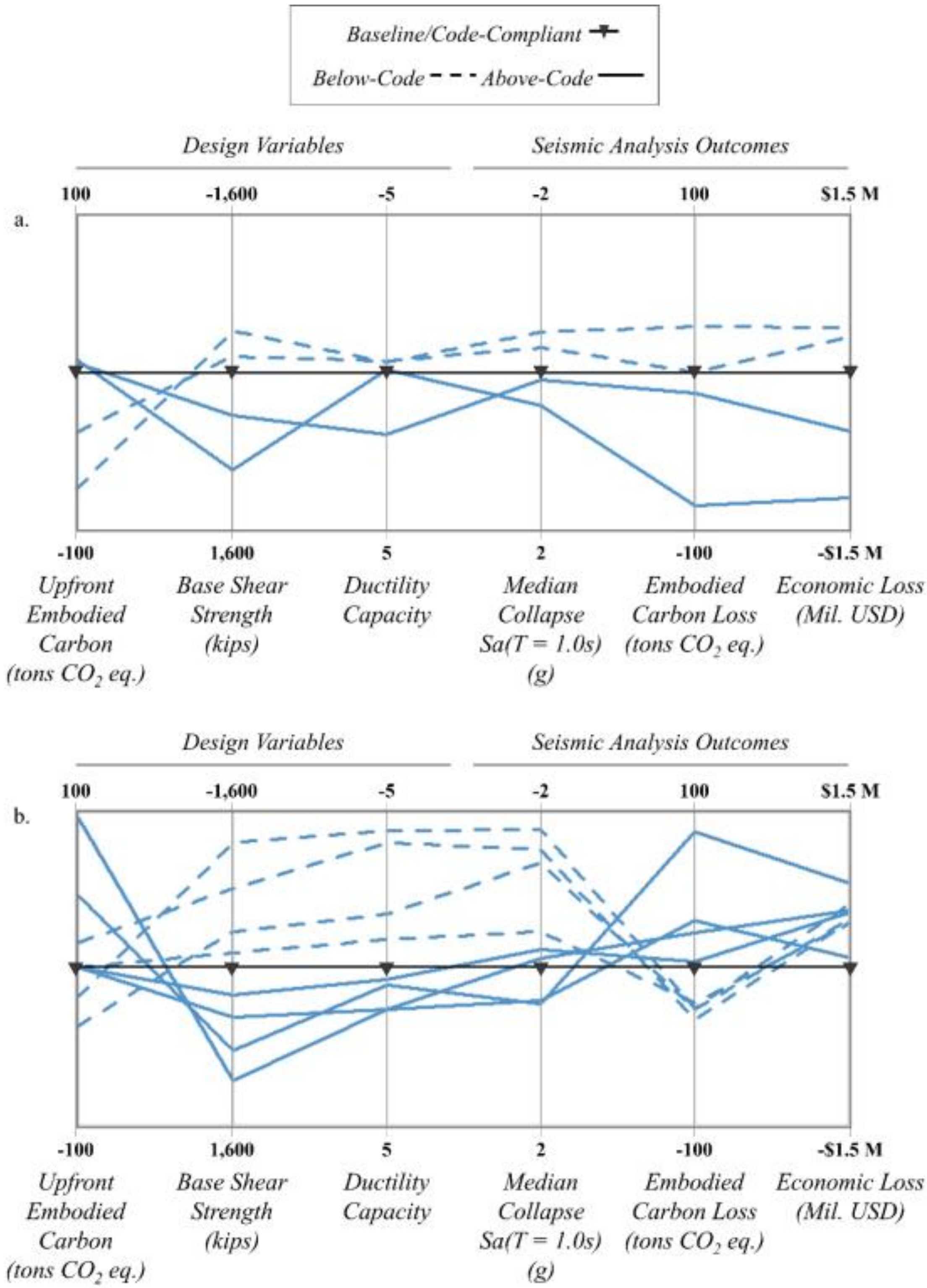

Fig. 11. Multi-objective analysis results comparing design and analysis outcomes for 4-story space frame a) strength design buildings and b) ductility design buildings. Results are presented with respect to a selected "baseline" design (code-compliant 4-story space frame), i.e. the value associated with the baseline design is subtracted from the value for the design of interest. Metrics are plotted on y-axis such that less desirable outcomes are at the top and more desirable are at the bottom.

Conclusions

This study investigates the idea that designing "green" buildings to withstand higher earthquake and other extreme loads offers a potential tool to reduce environmental impacts associated with post-hazard repairs. To do so, seismic performance and life-cycle embodied carbon are quantified for 30 RC buildings varying by lateral strength, ductility capacity, frame type, and height using nonlinear dynamic simulation and probabilistic loss assessment.

Changes in structural member sizes to vary design lateral strengths or ductility capacities influence upfront embodied carbon, which increases with enhanced lateral strength and, more so, with enhanced ductility capacity. Higher lateral strengths decrease economic seismic losses, but increase non-collapse, nonstructural loss contributions. Trends from enhanced ductility with respect to seismic losses are inconclusive; although improved ductility reduces the magnitude of collapse-induced costs relative to code-level designs, it also increases non-collapse, nonstructural losses. These trends apply to both the 4-story and 12-story buildings examined here.

This study quantifies the life-cycle (total) environmental impacts from seismic losses in terms of the embodied carbon associated with post-earthquake repair and replacement activities. The findings show that increasing lateral strength reduces total embodied carbon seismic losses. Trends in seismic losses for ductility designs are less clear because embodied carbon losses relate to the percentage and magnitude of contribution from non-collapse versus collapse losses; collapse losses tend to decrease with higher ductility capacity, but at the expense of larger non-collapse losses. Improved ductility capacity is thus less successful at achieving more resilient or greener life-cycle outcomes.

In conclusion, we find that increases in upfront embodied carbon required to achieve enhanced lateral strength can be offset by significant reduction in future post-earthquake losses, for a net savings in embodied carbon. Thus, this study demonstrates that enhancing lateral strength is a possible design tool for achieving greener buildings. These benefits from enhanced strength will be more significant in regions of high seismicity. The decision to enhance lateral strength above code-mandatory levels to achieve “green” goals will depend on the desired life-cycle objectives of a designer, but offers a possible avenue for incorporating principles of hazard-resistance into green building rating systems. For example, structures in regions with significant seismic, or other extreme load, hazard risks could be credited by demonstrating capacity increases above the code-minimum specifications. Future work on this topic could also expand the analysis presented herein to quantify total impacts (considering all life-cycle stages) of a building designed to achieve jointly performance-based goals for hazard-resistance and objectives for green building rating system standards. The overall findings of this study suggest a need in building design and analysis for holistic consideration of both economic and environmental impacts through life-cycle assessment of seismic losses.

Acknowledgments

This research is made possible through the support of the National Science Foundation (NSF), Grant #1234503. Any opinions, findings, and recommendations expressed are those of the authors and do not necessarily reflect the views of NSF. The authors gratefully acknowledge the Haselton Baker Risk Group for providing access to the SP3 software, as well as the contributions of two anonymous reviewers. In addition, discussions with Wil Srubar III, Joseph Kasprzyk, and Sherri Cook were helpful in developing the ideas herein.

References

ACI 318. (2011). *Building code requirements for structural concrete (ACI 318-11) and commentary (ACI 318R-11).* Farmington Hills, MI: American Concrete Institute.

Anagnos, T., Comerio, M. C., & Stewart, J. P. (2016). Earthquake Loss Estimates and Policy Implications for Nonductile Concrete Buildings in Los Angeles. *Earthquake Spectra*, *32*(4), 1951–1973.

Arroyo, D., Ordaz, M., & Teran-Gilmore, A. (2015). Seismic Loss Estimation and Environmental Issues. *Earthquake Spectra*, *31*(3), 1285–1308.

ASCE. (2010). *Minimum design loads for buildings and other structures: ASCE/SEI 7-10*. Reston, VA: American Society of Civil Engineers.

ATC. (2012a). *Seismic Performance Assessment of Buildings. Volume 1 - Methodology* (Vol. 1). Redwood City, CA: Applied Technology Concil.

ATC. (2012b). *Seismic Performance Assessment of Buildings. Volume 2 - Implementation Guide* (Vol. 2). Redwood City, CA: Applied Technology Concil.

Baker, J. W., & Cornell, C. A. (2003). *Uncertainty Specification and Propagation for Loss Estimation Using FOSM Methods*. Berkeley, CA.

Bocchini, P., Frangopol, D. M., Ummenhofer, T., & Zinke, T. (2014). Resilience and Sustainability of Civil Infrastructure : Toward a Unified Approach. *Journal of Infrastructure Systems*, *4014004*, 1–16.

CEC. (2008). Green Building in North America. In *Secretariat Report to Council under Article 13 of the North American Agreement on Environmental Cooperation*. Commission for Environmental Cooperation. Retrieved from www.cec.org/Storage/61/5386_GB_ Report_EN.pdf

Ching, E. (2014). *Building construction illustrated*. Hoboken, New Jersey: Wiley.

Chiu, C. K., Chen, M. R., & Chiu, C. H. (2013). Financial and Environmental Payback Periods of Seismic Retrofit Investments for Reinforced Concrete Buildings Estimated Using a Novel Method. *J. Archit. Eng.*, *19*(2), 112–118.

Court, A., Simonen, K., Webster, M., Trusty, W., & Morris, P. (2012). Linking Next-Generation Performance-Based Seismic Design Criteria to Environmental Performance (ATC-86 and ATC-58). In *Structures Congress 2012* (pp. 922–928).

Cowing, M. M., Pate, M. E., & Glynn, P. W. (2004). Dynamic modeling of the tradeoff between productivity and safety in critical engineering systems. *Reliability Engineering and System Safety*, *86*, 269–284.

Davis, M., & Porter, K. (2016). The Public's Role in Seismic Design Provisions. *Eathquake Spectra, In Press*.

EPA. (2008). Life Cycle Assessment: Principles and Practice. *U.S. Environmental Protection Agency*.

Feese, C., Li, Y., & Bulleit, W. M. (2014). Assessment of Seismic Damage of Buildings and Related Environmental Impacts. *J. Perform. Constr. Facil.*, *29*(4), 1–10.

Goedkoop, M., Oele, M., Leijting, J., Ponsioen, T., & Meijer, E. (2013). *Introduction to LCA with SimaPro*. Amersfoort, The Netherlands: PréSustainability.

Goulet, C. A., Haselton, C. B., Mitrani-reiser, J., Beck, J. L., Deierlein, G. G., Porter, K. A., & Stewart, J. P. (2007). Evaluation of the seismic performance of a code-conforming reinforced-concrete frame building — from seismic hazard to collapse safety and economic losses. *Earthquake Engng Struct. Dyn.*, *36*, 1973–1997.

Guggemos, A. A., & Horvath, A. (2005). Comparison of Environmental Effects of Steel- and Concrete-Framed Buildings. *Journal of Infrastructure Systems*, *11*(2), 93–101.

Hammond, G. P., & Jones, C. I. (2006). *Inventory of Carbon and Energy (ICE), Version 1.5a Beta*. Bath, UK.

Hammond, G. P., & Jones, C. I. (2008). Embodied energy and carbon in construction materials. *Energy*, *161*(2), 87–98.

Haselton, C. B., & Deierlein, G. G. (2007). *Assessing Seismic Collapse Safety of Modern Reinforced Concrete*

Moment Frame Buildings. Palo Alto, CA.

Haselton, C. B., Liel, A. B., Deierlein, G. G., Dean, B. S., & Chou, J. H. (2011). Seismic Collapse Safety of Reinforced Concrete Buildings. I: Assessment of Ductile Moment Frames. *Journal of Structural Engineering*, *137*(4), 481–491.

Haselton, C. B., Liel, A. B., Taylor-Lange, S. C., & Deierlein, G. G. (2016). Calibration of Model to Simulate Response of Reinforced Concrete Beam-Columns to Collapse. *ACI Structural Journal*, *113*(6), 1141–1152.

Haselton Baker Risk Group. (2016). Seismic Performance Prediction Program. Retrieved from http://www.hbrisk.com/

Hendrickson, C., Horvath, a, Joshi, S., & Lave, L. (1998). Economic input-output models for environmental life-cycle assessment. *Environmental Science & Technology*, *32*, 184a–191a.

Hossain, K. A., & Gencturk, B. (2014). Life-Cycle Environmental Impact Assessment of Reinforced Concrete Buildings Subjected to Natural Hazards. *J. Archit. Eng.*, *A4014001*(In Press).

Ibarra, L. F., Medina, R. a., & Krawinkler, H. (2005). Hysteretic models that incorporate strength and stiffness deterioration. *Earthquake Engineering & Structural Dynamics*, *34*(12), 1489–1511.

ICC. (2009). *2009 international building code*. Country Club Hills, IL.: International Code Council.

Jacquet, J., Hagel, K., Hauert, C., Marotzke, J., Röhl, T., & Milinski, M. (2013). Intra- and intergenerational discounting in the climate game. *Nature Climate Change*, *3*(12), 1025–1028.

Kajikawa, Y. (2008). Research core and framework of sustainability science. *Sustainability Science*, *3*(2), 215–239.

Liel, A. B., & Deierlein, G. G. (2013). Cost-Benefit Evaluation of Seismic Risk Mitigation Alternatives for Older Concrete Frame Buildings. *Earthquake Spectra*, *29*(4), 1391–1411.

Moehle, J. P., Hooper, J. D., & Lubke, C. D. (2008). *Seismic design of reinforced concrete special moment frames: a guide for practicing engineers. NEHRP Seismic Design Technical Brief No. 1*. Gaithersburg, MD. Retrieved from http://nvlpubs.nist.gov/nistpubs/gcr/2008/gcr08-917-1.pdf

Padgett, J., & Li, Y. (2016). Risk-Based Assessment of Sustainability and Hazard Resistance of Structural Design. *J. Perform. Constr. Facil.*, *30*(2).

Pate-Cornell, M. E. (1984). Discounting in risk analysis: capital vs. human safety. In M. Grigoriu (Ed.), *Risk, structural engineering and human error*. Waterloo, Canada: University of Waterloo.

PEER. (2014). The open system for earthquake engineering simulation. Retrieved from www.opensees.berkeley.org

Petersen, M. ., Frankel, A. D., Harmsen, S. C., Mueller, C. S., Haller, K. M., Wheeler, R. L., … Rukstales, K. S. (2008). *Documentation for the 2008 Update of the United States National Seismic Hazard Maps*.

Porter, K. (2003). An overview of PEER's performance-based earthquake engineering methodology. In *Ninth International Conference on Applications of Statistics and Probability in Civil Engineering (ICASP9)*. San Francisco, CA: Civil Engineering Risk and Reliability Association (CERRA).

Porter, K. A. (2016). Safe Enough ? A Building Code to Protect Our Cities and Our Lives. *Eathquake Spectra*, *32*(2), 677–695.

Portland Concrete Association. (2012). Functional Resilience: Prerequisite for Green Buildings. Retrieved from www.sustainableconcrete.org

Ramirez, C. M., Liel, A. B., Haselton, C. B., Mitrani-Reiser, J., Haselton, C. B., Spear, A. D., … Miranda, E. (2012). Expected earthquake damage and repair costs in reinforced concrete frame buildings. *Earthquake Engineering & Structrual Dynamics*, *41*(11).

Rodriguez-Nikl, T. (2015). Linking disaster resilience and sustainability. *Civil Engineering and Environmental Systems*, *32*(1–2), 157–169.

Ryan, K., Sayani, P., Baez, Y., & Mitrani-Reiser, J. (2009). Comparative Life Cycle Performance Assessment of Conventional and Seismic Isolated Buildings. In *International Symposium on Seismic Response Controlled Buildings for Sustainable Society, Tokyo, Japn*.

Sarkisian, M., Brunn, G., Nasr, M., Hachem, M., & Hu, L. (2011). Predicting the Environmental Impact of Structures in Regions of High Seismic Risk. In *AEI 2011* (pp. 263–271).

Schelling, T. C. (1995). Intergenerational discounting. *Energy Policy*, *23*(4–5), 395–401.

Tapia, C., & Padgett, J. E. (2012). Examining the Integration of Sustainability and Natural Hazard Risk Mitigation into Life Cycle Analyses of Structures. *Structures Congress 2012*, 1929–1940.

Tol, R. S. J. (2011). The Social Cost of Carbon. *Annual Review of Resource Economics*, *3*, 419–443.

Vamvatsikos, D., & Cornell, C. A. (2002). Incremental dynamic analysis. *Earthquake Engineering & Structural Dynamics*, *31*(3), 491–514.

Vamvatsikos, D., & Cornell, C. A. (2006). Direct estimation of the seismic demand and capacity of oscillators with multi-linear static pushovers through IDA. *Earthquake Engineering and Structural Dynamics*, *35*(9), 1097–1117.

Wei, H., Shohet, I. M., Skibniewski, J., & Shapira, S. (2016). Assessing the Lifecycle Sustainability Costs and Benefits of Seismic Mitigation Designs for Buildings. *J. Archit. Eng.*, *22*(1), 1–13.

Wei, H., Skibniewski, J., Shohet, I. M., & Yao, X. (2016). Lifecycle Environmental Performance of Natural-Hazard Mitigation for Buildings. *J. Perform. Constr. Facil.*, *30*(3), 1–13.

Welsh-Huggins, S. J., & Liel, A. B. (2016). A Life-Cycle Framework for Integrating Green Building and Hazard-Resistant Design: Examining the Seismic Impacts of Buildings with Green Roofs. *Structure and Infrastructure Engineering*, *13*(1), 19–33.